THE JOURNAL OF PHYSICAL CHEMISTRY A

pubs.acs.org/JPCA Article

# Coexistence of Left- and Right-Handed 12/10-Mixed Helices in Cyclically Constrained β-Peptides and Directed Formation of Single-Handed Helices upon Site-Specific Methylation

Karl N. Blodgett, Geunhyuk Jang, Sojung Kim, Min Kyung Kim, Soo Hyuk Choi,* and Timothy S. Zwier*

Cite This: J. Phys. Chem. A 2020, 124, 5856−5870 Read Online

ACCESS | Metrics & More | Article Recommendations | Supporting Information

**ABSTRACT:** The inherent conformational preferences of the neutral β−peptide foldamer series, Ac-$(ACHC)_n$-NHBn, $n$ = 2−4, are studied in the gas phase using conformation-specific IR−UV double resonance methods. The cyclically constrained chiral β-amino acid *cis*-2-aminocyclohexane carboxylic acid (ACHC) is designed to bring both right- and left-handed helices into close energetic proximity. Comparison of the infrared spectra in the NH stretch and amide I/II regions with the predictions of DFT calculations lead to the unambiguous assignment of four out of the six observed conformations of the molecules in this series, while corroborating computational and spectral evidence, affords tentative assignments of the remaining two conformers for which IR data were not recorded. The observed structures fall into one of two conformational families: a right-handed 12/10-mixed helix or its "cap-disrupted" left-handed helical analogue, which coexist with significant populations. Site-specific and stereospecific methylation on the cyclohexane backbone at the dipeptide ($n$ = 2) level is also tested as a means to sterically lock in a predetermined cyclohexane chair conformation. These substitutions are proven to be a means of selectively driving formation of one helical screw sense or the other. Calculated relative energies and free energies of all possible structures for the molecules provide strong supporting evidence that the rigid nature of the ACHC residue confers unusual stability to the 12/10-mixed helix conformation, regardless of local environment, temperature, or C-terminal capping unit. The simultaneous presence of both handed helices offers unique opportunities for future studies of their interconversion.

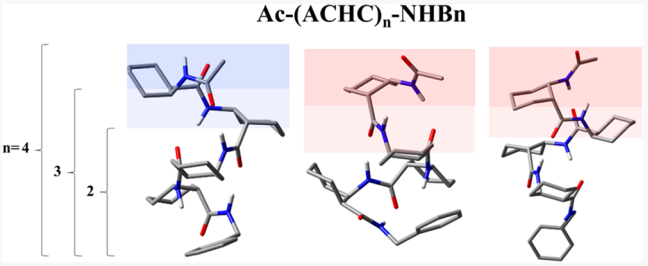




## I. INTRODUCTION

The secondary structures adopted by peptides result from a delicate balance of intermolecular and intramolecular interactions, including hydrogen bonding and amino-acid-specific steric effects. Among natural proteins, which are composed entirely of L-α-amino acid residues, the most common secondary structure is the helix, and the most common helices are the α-helix ($3.6_{13}$-helix) and the $3_{10}$-helix.[1−3] Due to their enantiomerically pure amino acid composition, natural peptides preferentially adopt either left- or right-handed helices, which are chiral with respect to one another.[4] Peptide sequences composed of achiral residues, however, have access to both left- and right-handed helical conformations, which may rapidly interconvert with one another in solution.[5−7] The helical screw sense of such peptides has been shown to be controllable by environmental factors such as temperature and interaction with chiral molecules. Several research groups are devoting effort to leveraging the environment-dependent helical screw sense of these molecules toward stimuli-responsive applications such as molecular recognition and catalysis.[4,8−11]

Since the first systematic studies of β-peptide helices by Gellman and Seebach, several helical structures not accessible to pure α-peptides have been identified, including the 12/10-, 10-, 8-, and 14-helices, where the number designates the number of atoms in the macrocycles enclosed by an NH···O=C H-bond.[12−16] Such synthetic foldamers have been shown to have diverse properties such as cholesteryl ester uptake inhibition, antimicrobial action, and the projection of carbohydrates into specific three-dimensional patterns.[17−21] In the past decade, the chiral β-amino acid, *cis*-2-aminocyclohexanecarboxylic acid (ACHC), shown in Figure 1, has received much attention as a foldamer building block.[1,6,7,15,22−26] The cyclically constrained nature of its six-membered ring demands that the ACHC residue adopt one of

Received: April 21, 2020
Revised: June 2, 2020
Published: June 4, 2020





https://dx.doi.org/10.1021/acs.jpca.0c03545
J. Phys. Chem. A 2020, 124, 5856−5870

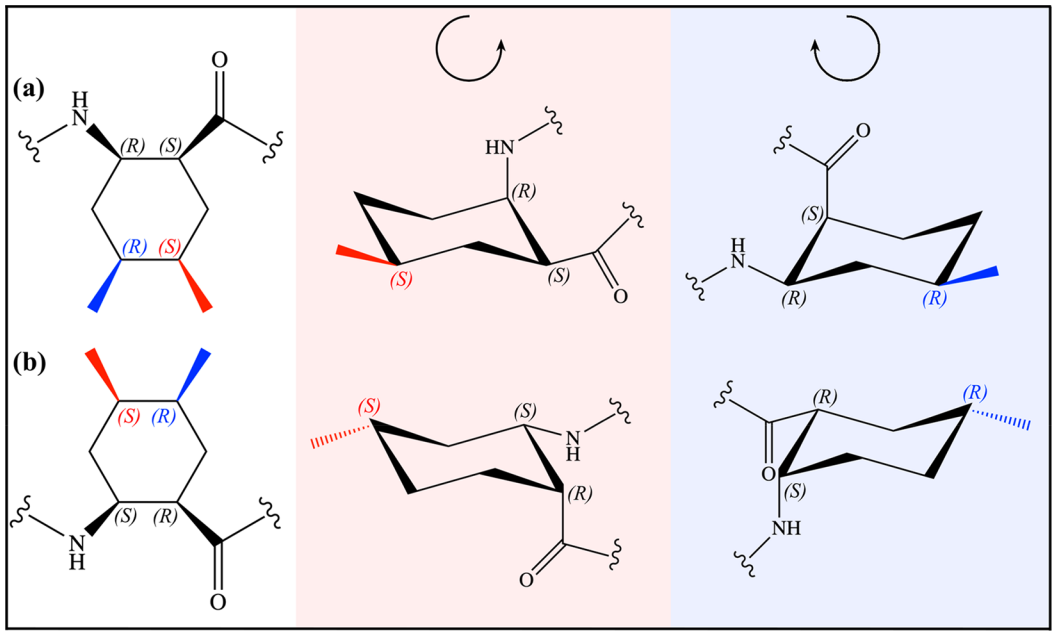


**Figure 1.** (a) *RS* and (b) *SR* *cis*-2-aminocyclohexanecarboxylic acid (ACHC) monomers used as the foldamer building blocks of the molecules studied in this work. Stereospecific and site-specific methylation along the cyclohexane backbone of each species drives the local conformation of the ACHC residue into a chair conformation in which the methyl group is in the energetically favored equatorial position. These steric constraints serve to orient the peptide backbone into either a left- or right-handed conformation. Note that each nonmethylated ACHC enantiomer may adopt either chair conformation.

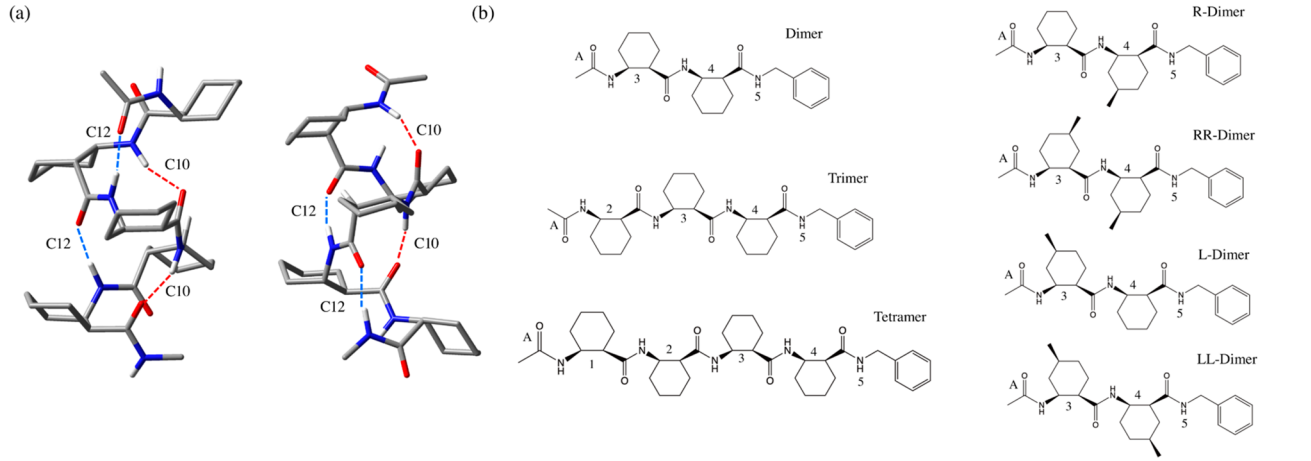


**Figure 2.** (a) Ac-(ACHC)$_5$-NHMe molecule in the left-handed (left) right-handed (right) 12/10 mixed-helical conformation with intramolecular hydrogen bonds labeled and color-coded as red (N → C terminal) or blue (C → N terminal). Structures taken from Shin et al.[6] (b) Chemical structures of the seven molecules studied in this work. Each residue is labeled, including the C-terminal NHBn cap (residue 5), and the N-terminal Acyl cap (residue A), such that the shared C-terminal motif composed of residues 3, 4 ,and 5 may be referred to in a coherent manner across all molecular species.

two energetically stable chair conformations: one in which the NH group is equatorial (eq) and the carbonyl group is axial (ax), or *vice versa*.

Temperature-dependent $^1$H NMR data from Shin et al. and Jang et al. showed that tetramer and pentamer oligomers composed of alternating enantiomers of ACHC units result in an equilibrium of left- and right-handed 12/10-mixed helices in chloroform, with left:right ratios of 2:1 and 4:1, respectively.[6,7] The 12/10 mixed helix, shown in Figure 2, is composed of hydrogen bonds oriented in alternating directions, N → C terminal and C → N terminal. The antiparallel alignment of hydrogen bonds along the helical axis results in a small net dipole moment relative to the macrodipoles acquired by the ubiquitous $\alpha$- and $3_{10}$-helices in $\alpha$-peptides. Such mixed helices are common in $\beta$-, $\gamma$-, $\alpha/\beta$-, and $\alpha/\gamma$-peptides but are quite rare in naturally occurring proteins.[27,28]

That the ACHC oligomer demonstrates reversible helical handedness in solution despite being composed of chiral residues is a remarkable fact that may be understood by viewing each oligomer as being composed, not of alternating chiral ACHC residues, but of repeating "pseudo-symmetric" achiral dimer units, composed of two ACHC residues of opposite chirality (*RS* and *SR*). The cyclohexane ring flip of both ACHC residues in one such dimer unit results in a left-handed (right-handed) motif inverting to its right-handed (left-handed) counterpart, where each dimer may be thought


https://dx.doi.org/10.1021/acs.jpca.0c03545
J. Phys. Chem. A 2020, 124, 5856−5870

of as achiral. Similarly, the cooperative cyclohexane ring flip of all ACHC moieties along a peptide backbone, where all chair conformations are inverted, results in the unwinding of the helix from one screw sense while reforming the other screw sense, i.e., from left → right, or right → left-handed helices.

The conformations that isolated molecules adopt are free from perturbative solvent and intermolecular interactions present in solution and crystal environments. As a result, the constituent-specific intramolecular interactions and steric effects act in an unencumbered fashion to drive conformational preferences. Laser spectroscopy of isolated, expansion-cooled molecules enables the study of these inherent conformational preferences at a spectral resolution sufficient for recording single-conformation spectra. In this manuscript, we study the conformational preferences inherent to a series of neutral ACHC-containing $\beta$-peptides, Ac-$(ACHC)_n$-NHBn, $n$ = 2, 3, 4, using IR−UV double-resonance spectroscopy in conjunction with supersonic cooling in the gas phase. The structures of the three molecules that make up this fundamental series are shown in the middle of Figure 2.

Additionally, we investigate the effect that substitution of a methyl group at selected positions on the cyclohexane ring has on driving a particular helical screw sense at the dipeptide level. As shown in Figure 1, orientation of the ACHC residue by methyl substitution in the energetically and sterically favored equatorial position predisposes the peptide backbone toward either left- or right-handed helical formation. Choi and co-workers have shown that incorporation of a specific methylated residue at every other ACHC unit in the tetramer or pentamer efficiently locks in a particular helical screw sense in solution.[6,7] Herein, we investigate the conformational effect that one or two such residues have on driving conformational preferences toward a particular handed helix. The structures of these substituted dipeptides are shown in the right column of Figure 2.

As we will see, the conformations of the seven molecules shown in Figure 2 fall into just two unique helical secondary structures, implying that the ACHC residue effectively organizes itself and the peptide backbone into its preferred structure at the dipeptide level, where additional residues build on and extend the existing structural motif.

## II. METHODS

**II.A. Experimental Methods.** The synthetic procedure for the molecules studied herein is found in the Supporting Information. The experimental procedure for recording single-conformer spectra has been described in detail elsewhere.[1,29] The solid state sample is desorbed from a thin film rubbed onto the surface of a translatable graphite rod placed directly below the pulsed valve orifice. Further details of the laser desorption procedure is given in the Supporting Information.

Resonant two-photon ionization (R2PI) was used to record the non-conformer-specific UV excitation spectra for all molecules. The frequency-doubled 20 Hz output of a tunable dye laser (Radiant Dyes, NarrowScan), pumped by the third harmonic of a Q-switched Nd:YAG laser (Continuum Surelite II) was scanned across the $S_0$−$S_1$ origin region (37 000−37 800 $cm^{-1}$) of the NHBn chromophore. Mass-selected ion signal at the molecular ion mass was plotted against the excitation wavelength to generate the one-color R2PI spectrum.

Conformation-specific IR spectra were recorded in the hydride stretch (3200−3500 $cm^{-1}$, 12−15 mJ/pulse) and amide I/II (1400−1800 $cm^{-1}$, 500−1000 $\mu$J/pulse) regions using resonant ion-dip infrared (RIDIR) spectroscopy.[30] The 10 Hz output of a Q-switched Nd:YAG pumped KTP/KTA-based IR optical parametric converter (LaserVision) temporally precedes by 100 ns, and spatially overlaps with, the UV laser, which has its wavelength fixed on some vibronic transition unique to one conformer in the molecular beam. A gated integrator (Stanford Research) acting in active baseline subtraction mode captures the 20 Hz ion signal generated by the UV laser. When the IR laser is resonant with a vibrational transition of the same conformer being monitored by the UV laser, ground state population of that conformer is removed, resulting in a subsequent dip in the UV-generated ion signal. This difference signal is output from the gated integrator and plotted as a function of IR frequency. IR radiation in the amide I/II regions was generated by difference frequency mixing the signal and idler output of the optical parametric converter in a $AgGaSe_2$ crystal.

With R2PI and RIDIR spectra in hand, the non-conformer-specific R2PI spectrum may be decomposed into its component parts using IR−UV holeburning (HB) spectroscopy. This scheme is identical to RIDIR spectroscopy, except that now the IR wavelength is fixed on some conformer-specific vibrational transition while the UV laser is scanned across the $S_0$−$S_1$ absorption region. Fractional ion signal depletion is plotted as a function of UV wavelength, resulting in single-conformation UV spectrum.

**II.B. Computational Methods.** The conformational landscapes of the molecules studied herein were initially explored within the MACROMODEL suite of programs using a torsional-sampling Monte Carlo Multiple Minimum algorithm in conjunction with the OPLS3 and Amber* force fields.[31] Exhaustive searches were performed with each force field such that additional searching yielded no new structures. Redundant conformer elimination performed on the group of structures from both OPLS3 and Amber* force fields calculated to lie within 50 kJ/mol of their respective global minimum generated starting structures for further DFT optimization.

Density functional theory within the Gaussian16 computational package was used to perform geometry optimizations and normal-mode frequency calculations on each candidate structure.[32] The Becke 3LYP hybrid functional was used in conjunction with Grimme's dispersion correction[33] (version D3), Becke−Johnson damping,[34] and the 6-31+G(d) Pople basis set. An ultrafine grid and tight convergence were used to ensure reliable normal-mode frequencies to be compared with experimental values. Scale factors of 0.958, 0.982, and 0.970 were used in the hydride stretch, amide I, and amide II regions to correct for anharmonicity of the calculated harmonic normal modes.

**II.C. Nomenclature.** The named molecules studied in this work are shown in Figure 2. The dimer, trimer, and tetramer are so named because they are composed of two, three, and four ACHC residues. The four additional dimers include either L (left) or R (right) in front of their name. These represent the helical screw sense in which they have been engineered to turn (see Figure 1). As can be seen, the dimers with one methylated ACHC ring use a single letter (R or L) to specify them, while those dipeptides with both ACHC groups methylated are named RR or LL. A "C$n$" notation is used to describe hydrogen bonded cycles, where $n$ represents the number of atoms involved in the ring closed by an NH···O═C H-bond. $\pi$


https://dx.doi.org/10.1021/acs.jpca.0c03545
J. Phys. Chem. A 2020, 124, 5856−5870

H-bonds are labeled "$\pi$", and NH groups not involved in H-bonding are labeled "F" for free. Our labeling scheme describes the interaction of each amide NH group along the peptide backbone, going from the N to the C terminus. Additionally, each residue is labeled, including the C-terminal NHBn cap (labeled residue 5), and the N-terminal Acyl cap (labeled residue A), such that the C-terminal motif composed of residues 3, 4, and 5, which is common among all molecules studied here, may be referred to in a coherent manner across all molecular species. In the assigned 2D and 3D structures, blue dashed lines represent C → N-terminal (NH→O═C) directed hydrogen bonds, while red dashed lines represent N → C-terminal directed hydrogen bonding. Backbone dihedral angles $\varphi$, $\theta$, and $\psi$ are defined in the conventional manner.

## III. RESULTS AND ANALYSIS

**III.A. Dimer, R-Dimer, and RR-Dimer.** *III.A.1. R2PI and IR−UV HB Spectroscopy.* R2PI and IR−UV HB spectra for the dimer are show in Figure 3a. The IR−UV HB spectrum

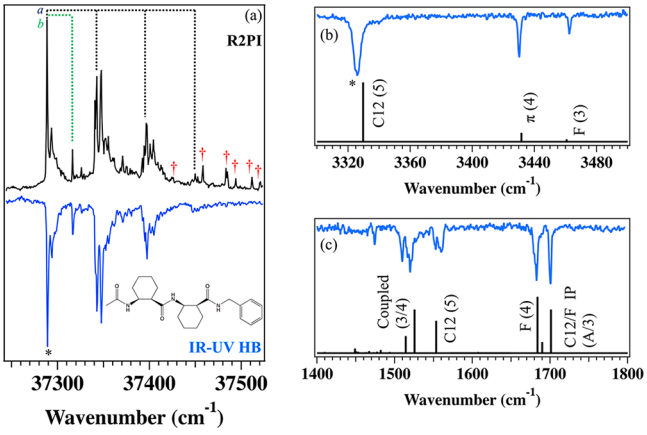


**Figure 3.** (a) R2PI and IR−UV HB spectra in the $S_0$−$S_1$ region of the dimer. Franck−Condon progressions marked with *a* and *b* correspond to low-frequency modes of 54 and 27 cm$^{-1}$, respectively. Red daggers mark peaks belonging to a conformation with minor population in the expansion while peaks marked with an asterisk were used to collect holeburn spectra. (b) and (c) RIDIR spectra of the dimer in the hydride stretch and amide I/II regions, respectively. Stick spectra below each experimental trace represent the scaled, harmonic normal-mode frequencies of the assigned conformation. These vibrational transitions, calculated at the B3LYP-D3BJ/6-31+G(d) level of theory, are labeled with the main carrier(s) of the vibration.

recorded with the IR HB laser fixed at 37 288 cm$^{-1}$ shows that most of the peaks in the R2PI spectrum belong to one major conformer. The remaining peaks, marked with red daggers, likely belong to some minor conformer in the jet with a small population. Insufficient signal prohibited further investigation of this minor conformer. The major conformer has its $S_0$−$S_1$ origin transition at 37 288 cm$^{-1}$, with Franck−Condon progressions up to $\nu$ = 3 in a 54 cm$^{-1}$ mode, and $\nu$ = 1 in a 27 cm$^{-1}$ mode. According to the calculated vibrational frequencies of the assigned structure (see section III.A.2), these low-frequency modes correspond to the absorbing phenyl ring rocking against NH[4] and ACHC[3]. Additionally, the members of the 54 cm$^{-1}$ mode progression have a 5 cm$^{-1}$ transition built off them. These peaks are likely sequence bands of the same mode originating from $\nu$ = 1 in the ground state, whose corresponding $S_1$ frequency is 5 cm$^{-1}$ larger. Sequence bands such as these are common among laser-desorbed species due to incomplete cooling to their zero-point vibrational level.[35−37]

The R- and RR-dimers have UV and IR spectra nearly identical to those of the dimer. Their $S_0$−$S_1$ origin transitions are shifted down by 1 and 3 cm$^{-1}$, respectively, from that of the dimer. Even smaller shifts are found in their recorded IR spectra (see Figures S7 and S8 for the UV and IR spectra of the R- and RR-dimers). Therefore, the UV and IR spectra of the R- and RR-dimers will not be discussed in detail. One important difference, however, is that the UV spectra of both the R- and RR-dimers are composed entirely of transitions from one conformer, whereas the dimer contains small contributions from a second minor conformer. This point will be returned to in section III.B.1.

*III.A.2. RIDIR Spectroscopy.* Panels b and c of Figure 3 present the RIDIR spectra of the major conformer of the dimer in the NH and amide I/II regions, respectively. In anticipation of observing 12/10 mixed-helices, we should be on the lookout for their characteristic spectral features. The structure of the 12/10-helix in Figure 2a shows two free NH groups, which are in positions such that the addition of one ACHC residue on the N- and C-terminus of the helix would result in new C12 and C10 H-bonds, respectively, that grow the helix in either direction. One would anticipate, then, as a signature of the 12/10-helix, two free NH stretch transitions in the IR spectrum, with the remaining transitions resulting from NH groups involved in C10 and C12 H-bonds. The C-terminal NHBn cap with which our molecules have been modified, however, can interfere with the repeating helical pattern.

There are many previous examples of NH···$\pi$ interactions in the conformational makeup of aromatic ring-containing molecules in the gas phase.[24,35,36,38,39] Calculations suggest that the right-handed 12/10-helix will have one free NH near the N-terminus, and the NH[4] involved in dispersive interactions with the $\pi$-cloud of the phenyl ring. The left-handed 12/10-helix, however, is expected to take up a configuration in which dispersive interactions with the $\pi$-cloud are not possible, resulting in two free NH groups, one on either end of the helix. Calculations suggest, however, that this helical purity may be disrupted by forming the NH[5]···O═C[3] C8 and NH[3]···$\pi$ interactions rather than the NH[3]···O═C[4] C10 H-bond of the "pure" left-handed helix. We keep these considerations in mind as we analyze the following spectra.

As mentioned in the previous section, the spectra of the dimer are nearly identical with those of the R- and RR-dimers. In discussing one, then, we discuss them all. The dimer shows two high-frequency NH stretch transitions at 3462 and 3430 cm$^{-1}$, and an intense, broadened transition at 3326 cm$^{-1}$. The weak, highest frequency band shows up where one would expect a free NH stretch to appear, while the 3430 cm$^{-1}$ band is consistent with formation of an NH···$\pi$ bond with the aromatic ring.[1,24,38] Evidence for this NH···$\pi$ interaction is provided by the low-frequency Franck−Condon activity in the UV spectra of this triad of molecules. Red-shifted, broadened, intense infrared bands are generally understood to arise from NH groups involved in strong hydrogen bonding interactions. On the basis of the hydride stretch spectra alone, one would anticipate a structure with one free, one $\pi$-interacting, and one strongly hydrogen bonded NH, which, on the basis of the considerations discussed above, we tentatively assign to an emergent form of the right-handed 12/10-helix.


https://dx.doi.org/10.1021/acs.jpca.0c03545
J. Phys. Chem. A 2020, 124, 5856−5870

The calculated spectra, shown as black sticks in Figure 3, capture both the relative intensity and frequency of all recorded IR transitions to a remarkable degree. The structure corresponding to the stick spectra, as well as a 2D sketch of the hydrogen bonding pattern, is shown in Figure 4a. This

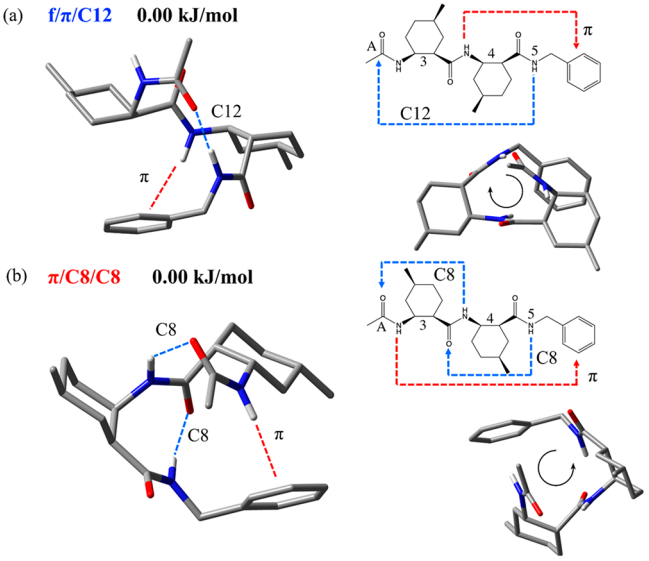


**Figure 4.** Assigned structures and relative zero-point-corrected potential energies of (a) the dimer, R-dimer, and RR-dimer and (b) the L-dimer and LL-dimer. In each case, the doubly methylated dipeptide is used to illustrate the steric control by which the methyl residues dictate local ACHC conformation. 2D hydrogen-bonding schematics are presented for each molecule, along with a down-axis view from N to the C terminus, highlighting the preferred screw sense of each dipeptide.

conformer was calculated to be the global minimum by DFT B3LYP-D3BJ/6-31+G(d) calculations for the R-dimer, RR-dimer, and dimer. From the assigned structure we can see that NH[3] is free, NH[4] is interacting with the $\pi$-cloud of the phenyl cap, and NH[5] is in a C12 hydrogen bond with C═O[A], resulting in the inception of a right-handed 12/10-helix, which is just long enough to make 1 full helical turn. The exact structure shown in Figure 4a is that of the RR-dimer, where one can see that the methyl groups on either ACHC ring are in the energetically favorable equatorial position, thereby sterically locking in the right-handed helical structure.

The amide I data from 1600−1800 $cm^{-1}$ in Figure 3c report on the C═O stretch vibrations, which generally shift to lower frequency upon accepting strong H-bonds. The amide II region from 1400−1600 $cm^{-1}$ is associated with the NH bend fundamentals, which generally shift up in frequency when in strong hydrogen bonds. However, due to the high degree of local-mode coupling, the amide II region is generally more difficult to interpret without the aid of calculations. The amide I data show a symmetric band at 1701 $cm^{-1}$ and a band with a high-frequency shoulder at 1683 $cm^{-1}$. According to calculations, the high-frequency band and the small shoulder belong to the in-phase and out-of-phase coupled stretches of the C═O[A] and [3] oscillators. The out-of-phase stretch has such a small intensity because the two C═O groups are oriented nearly antiparallel to one another, resulting in a small net change in dipole with respect to the coupled, out-of-phase stretch. The lowest frequency amide I band (1683 $cm^{-1}$) corresponds to the free C═O[4] stretch. The low frequency of this free C═O group may be understood by the fact that the NH on the same amide group is involved in the strong C12 H-bond, a scenario that is known to shift C═O stretch fundamentals to lower frequency.[37,40]

The amide II data show a split, high-frequency transition centered at 1557 $cm^{-1}$. The calculations predict that this transition is associated with the bend fundamental of NH[5], which is acting as donor in the C12 hydrogen bond. This band is likely split due to a 2:1 Fermi resonance with a mode with near half the frequency of the bend fundamental. Indeed, the calculated vibrations show several modes centered around this frequency, all of which include substantial wagging of NH[5]. It is interesting to note that in neither the R- or RR-dimer is this 1557 $cm^{-1}$ band split. This is likely due to the change in reduced mass shifting the overtone of the lower frequency vibration out of Fermi-resonance with this band. The two lower frequency amide II transitions shown in Figure 3c correspond to the coupled NH[3,4] bend fundamentals. Given the right-handed 12/10-helicity of the dimer, its IR spectra will be used as a reference to compare with other structures in what follows.

Figure 5a displays an energy level diagram for the dipeptides studied in this work. The horizontal lines represent the zero-

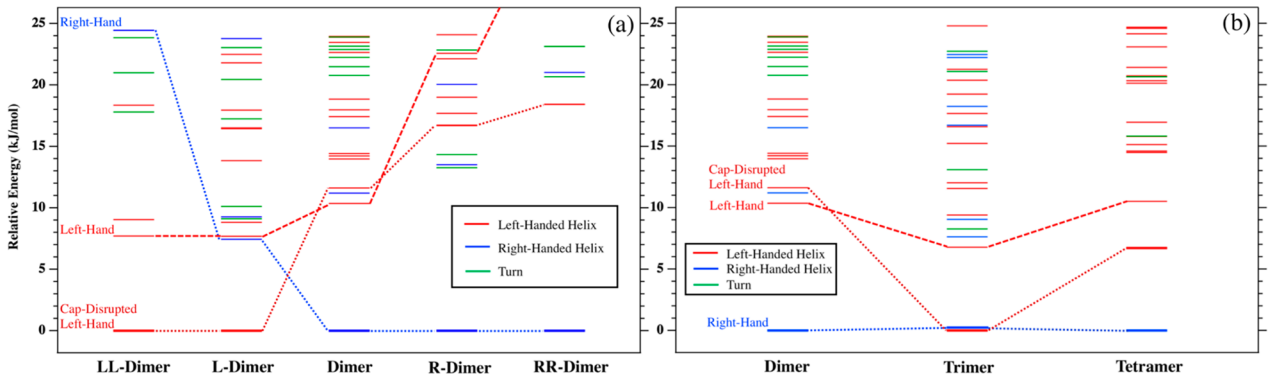


**Figure 5.** Energy level diagrams for (a) the set of methylated dipeptides and (b) the series Ac-$(ACHC)_n$-NHBn with $n$ = 2, 3, 4. Each conformational minima has its relative zero-point-corrected energy (B3LYP-D3BJ/6-31+G(d)) plotted as a horizontal bar and color-coded to represent left-handed (red), right-handed (blue), or general turned (green) structures. Experimentally assigned conformers are represented with a heavy horizontal bar. The "pure" right- and left-handed helices as well as the cap-disrupted helical structures are labeled and connected via dotted lines to their corresponding structures across the molecules.


https://dx.doi.org/10.1021/acs.jpca.0c03545
J. Phys. Chem. A 2020, 124, 5856−5870

point corrected energies for all structures calculated to lie within 25 kJ/mol of the global minimum. Lines are further color-coded to indicate the structural family to which each conformer belongs (red (left-handed helix), blue (right-handed helix), green (turned structures)), while the bold lines indicate the experimentally observed conformers. Note that each dipeptide contains all three structural families within 25 kJ/mol. While not assigned to any experimentally observed conformer in this work, the structure and calculated IR spectra of the lowest energy turned conformations at the $n = 2-4$ level are presented in Figure S9. We will return to the energy level diagram in the discussion. For now, we observe the 10.4 kJ/mol energy gap between the assigned global minimum right-handed helical structure of the dimer and the next lowest energy structure, which is an incipient form of the left-handed 12/10-helix.

**III.B. L-Dimer and LL-Dimer.** *III.B.1. R2PI and IR−UV HB Spectroscopy.* The R2PI and IR−UV HB spectra of the LL-dimer are shown in Figure 6a. The IR−UV HB spectrum indicates that all of the peaks in the R2PI spectrum are due to one conformer, which is a point of departure from the nonmethylated dimer. The sole conformer of the LL-dimer has its $S_0-S_1$ origin transition at 37 423 $cm^{-1}$, with Franck−Condon progressions up to $\nu = 4$ in 27 and 32 $cm^{-1}$ modes. The presence of combination bands involving these modes results in the increasing density of bands at higher frequencies. According to the calculated vibrational frequencies of the assigned structure (see section III.B.2), these modes correspond to the aromatic ring rocking against the NH[3] and the ACHC[3] ring. The weak band red-shifted by −20 $cm^{-1}$ from the origin is likely a hot band originating from a $\nu = 1$ populated level in the ground state and terminating in the zero-point level in $S_1$.

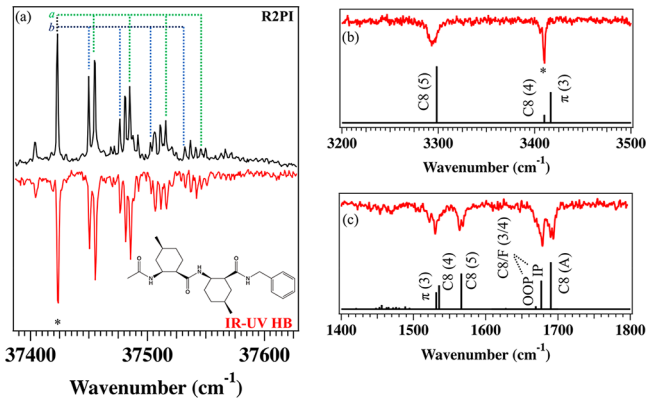


**Figure 6.** (a) R2PI and IR−UV HB spectra in the $S_0-S_1$ region of the LL-dimer. Franck−Condon progressions marked with *a* and *b* correspond to low-frequency modes of 32 and 27 $cm^{-1}$, respectively. (b) and (c) display the RIDIR spectra of the LL-dimer in the hydride stretch and amide I/II regions, respectively. Stick spectra below each experimental trace represent the scaled, harmonic normal-mode frequencies of the assigned conformation. These vibrational transitions, calculated at the B3LYP-D3BJ/6-31+G(d) level of theory, are labeled with the main carrier(s) of the vibration. Transitions marked with an asterisk were those used to collect holeburn spectra.

The L- and LL-dimers share nearly identical UV and IR spectra. The UV spectrum of the L-dimer has its $S_1$ origin transition shifted 4 $cm^{-1}$ higher in frequency to 37 427 $cm^{-1}$ and displays the same Franck−Condon activity and intensity pattern as the LL-dimer (see Figure S10 for the UV and IR spectra of the L-dimer). Given the similarity of the spectra, we do not discuss the L-dimer in detail in the main text. The $\pi\pi^*$ origin transition of the LL-dimer is shifted by about 135 $cm^{-1}$ to higher frequency than that of the RR-dimer, suggesting that the phenyl groups are in different environments between the two structures (see Figure S11 for a comparative plot of the R2PI spectra of all dipeptides studied herein). The minor peaks that did not burn out with the major conformer in the IR−UV HB spectrum of the nonmethylated dimer appear at the same frequencies as the UV transitions of the LL-dimer. This suggests that the minor conformation of the dimer is the same as that of the LL-dimer and is tentatively assigned as such. Energetic considerations bolster this argument (Figure 5a).

*III.B.2. RIDIR Spectroscopy.* Panels b and c of Figure 6 presents the RIDIR spectra of the LL-dimer in the NH and amide I/II regions, respectively. Two high-frequency bands of large and low intensity are present in the NH stretch spectrum at 3410 and 3405 $cm^{-1}$, respectively. This region may contain transitions from various types of weakly hydrogen bonded NH groups, rendering an *a priori* analysis of the spectrum difficult. The absence of transitions at higher frequencies indicates that there are no free NH groups in this conformer, and the broadened transition at 3293 $cm^{-1}$ is associated with the presence of one strong H-bond. Thus, one would anticipate a

**Table 1. Hydrogen Bond Distances (in Å) for All Assigned Structures Studied in This Work**[a]

| | NH no. | | | | |
|---|---|---|---|---|---|
| conformer | 1 | 2 | 3 | 4 | 5 |
| | | | Right-Hand 12/10 Mixed Helix | | |
| dimer | | | F | ~2.65 (π) | 1.87 (C12) |
| R-dimer | | | F | ~2.65 (π) | 1.87 (C12) |
| RR-dimer | | | F | ~2.65 (π) | 1.87 (C12) |
| trimer conf B | | 1.89 (C10) | F | ~2.56 (π) | 1.85 (C12) |
| tetramer conf B | F | 1.93 (C10) | 1.90 (C12) | ~2.56 (π) | 1.84 (C12) |
| | | | Cap-Disrupted Left-Hand 12/10 Mixed Helix | | |
| L-dimer | | | ~2.54 (π) | 2.22 (C8) | 1.92 (C8) |
| LL-dimer | | | ~2.54 (π) | 2.22 (C8) | 1.92 (C8) |
| trimer conf A | | F | ~2.55 (π) | 1.87 (C12) | 1.92 (C8) |
| tetramer conf A | 1.88 (C10) | F | ~2.65 (π) | 1.84 (C12) | 1.92 (C8) |

[a]Parameters were calculated at the B3LYP-D3BJ/6-31+G(d) level of theory.



https://dx.doi.org/10.1021/acs.jpca.0c03545
J. Phys. Chem. A 2020, 124, 5856−5870

structure in which there are two relatively weak, and one relatively strong, H-bond interactions.

The calculated IR spectra corresponding to the assigned structure, shown as black sticks below the experimental trace in Figure 6, replicate the experimental frequencies and intensities with high fidelity. The assigned structure corresponding to the stick spectra and a 2D sketch of the hydrogen bonding pattern are shown in Figure 4b. As seen in Figure 5a, this conformer was calculated to be the global minimum for both the L- and LL-dimers at the DFT B3LYP-D3BJ/6-31+G(d) level of theory. From the assigned structure we can see that NH[3] is interacting with the $\pi$-cloud of the phenyl cap, NH[4] and NH[5] are in C8 hydrogen bonds with C═O[A] and C═O[3], respectively, in forming a $\beta$-peptide analogue of a left-handed double $\gamma$-turn. The structure shown in Figure 4b is that of the LL-dimer, where one can see that the methyl groups on either ACHC ring are in the energetically favorable equatorial position, sterically locking in the local ACHC conformations.

This structure is clearly not the left-handed 12/10-helix, but it *is* the aforementioned cap-disrupted helix, where rather than a C10 H-bond, a structure is formed with C8 H-bonds at either terminus and an NH···$\pi$ H-bond at the C-terminus. This structure is energetically favored for both the L- and LL-dimers (Figure 5a), a point we will explore further in the Discussion. It is important to keep in mind that for longer sequences of Ac-(ACHC)$_n$-NHBn, where $n > 2$, the 12/10-helical hydrogen-bonding motif can coexist with cap-disrupted C-terminal C8 and $\pi$-hydrogen bonds, which serve as a helical capping unit. This will become more relevant in the following sections.

We note that the two NH stretch transitions corresponding to the pair of C8 H-bonds are separated by over 100 cm$^{-1}$ and are quite different in intensity. C8 H-bonds are the $\beta$-peptide analogue of C7 H-bonds in $\alpha$-peptides, the transition frequency of which can span ~200 cm$^{-1}$.[24,36,38,39] The H-bond distances shown in Table 1 provide a firm basis for the frequency difference in the two C8 H-bond lengths. The assigned structure of the LL-dimer has an NH[5]···O═C[3] H-bond distance (1.92 Å), 0.30 Å shorter than for NH[4]···O═C[A] distance (2.22 Å).

The amide I data from 1600 to 1800 cm$^{-1}$ in Figure 6c show a split, high-frequency band at 1692 cm$^{-1}$ and a lower frequency band with a low-frequency shoulder centered at 1679 cm$^{-1}$. The higher frequency transition corresponds to the C═O[A] group involved in the weaker C8 H-bond, while the two lower frequency transitions are due to in-phase and out-of-phase combinations of the C═O[3] and C═O[4] groups. The spectrum in the amide II region (1400−1600 cm$^{-1}$) shows a split peak at 1566 cm$^{-1}$, and a pair of peaks at lower frequencies of 1530 and 1522 cm$^{-1}$. On the basis of the relative strengths of the two C8 H-bonds, we would anticipate the higher frequency transition to correspond to the NH[5] bend, the middle frequency to the NH[4] bend, and the lower frequency to the NH[3] bend. The calculations bear this out. It is interesting to note that both the L- and LL-dimers display the same split bands in the amide I and II spectra, indicating a likely common Fermi resonance.

**III.C. Trimer.** *III.C.1. R2PI and IR−UV HB Spectroscopy.* The R2PI and IR−UV HB spectra of the trimer are shown in Figure 7a. Most of the peaks in the R2PI spectrum are accounted for in the IR−UV HB spectrum, with some exceptions: the peaks marked with blue daggers do not burn out with the same relative intensities with which they appear in the R2PI spectrum. This may be explained in one of two ways.

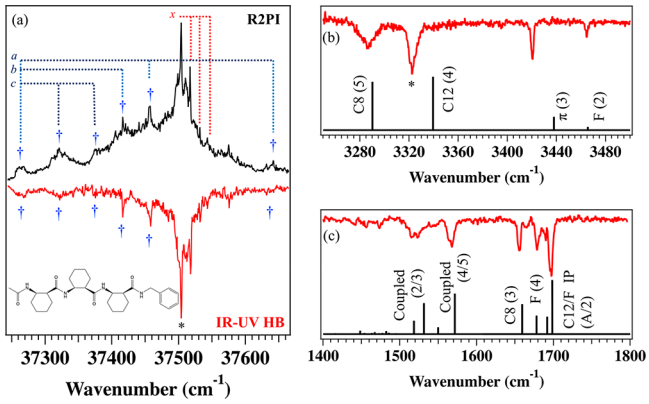


**Figure 7.** (a) R2PI (black) and conformer A IR−UV HB (red) spectra in the $S_0$−$S_1$ origin region of the trimer. Blue daggers mark peaks belonging to a minor conformation (conf B) in the molecular beam (see text for details). A Franck−Condon progression in the major conformation (conf A) marked with *x* corresponds to a low-frequency mode of 14 cm$^{-1}$, while *a*, *b*, and *c* correspond to low-frequency modes in conf B of 188, 151, and 27 cm$^{-1}$, respectively. (b) and (c) RIDIR spectra of conformer A in the hydride stretch and amide I/II regions, respectively. Stick spectra below each experimental trace depict the scaled, harmonic vibrational frequencies of the assigned conformation. These vibrational transitions, calculated at the B3LYP-D3BJ/6-31+G(d) level of theory, are labeled with the main carrier(s) of the vibration. Transitions marked with an asterisk were those used to collect hole-burn spectra.

If these peaks were due to hot or sequence band transitions, one might expect a decreased intensity pattern relative to the cold bands originating from the zero-point level in the hole burn spectrum due to shifting and broadening of the hot band IR absorption. A second possibility is that these peaks are due to another conformer in the molecular beam, which absorbs at the same IR frequency used to record the conformer-specific IR−UV HB spectra of the major conformer (the peak marked with an asterisk in the RIDIR spectra in Figure 7b). We will return to this point in section III.

The major conformer (conformer A) has its $S_0$−$S_1$ origin transition at 37 504 cm$^{-1}$, with sequence bands at higher and lower frequencies due to incomplete vibrational cooling, and a Franck−Condon progression up to $\nu = 3$ in a 14 cm$^{-1}$ mode. Vibrational analysis of the assigned structure (see next section) indicates that this mode is due to the rocking of the phenyl cap against the ACHC[3] and NH[3] groups.

*III.C.2. RIDIR Spectroscopy.* Panels b and c of Figure 7 present the RIDIR spectra of conformer A of the trimer in the NH stretch and amide I/II regions, respectively. We observe one weak, high-frequency NH stretch at 3464 cm$^{-1}$ and a more intense transition at 3420 cm$^{-1}$. Using similar logic as outlined above, we may tentatively assign these transitions to a free and a $\pi$-bound NH, respectively. Two broadened, lower frequency transitions appear at 3322 and 3286 cm$^{-1}$, in a region indicative of strong hydrogen bonds. We note the similarity between this spectrum and that of the LL-dimer and tentatively assign the low-frequency transition at 3286 cm$^{-1}$ to a C8 hydrogen bonded NH stretch fundamental. Similarly, we see that the NH stretch spectra of the RR-dimer has a comparably intense and broadened band at 3326 cm$^{-1}$ assigned to a C12 H-bond. We therefore tentatively assign the band at 3322 cm$^{-1}$ to a C12 H-bond.

The calculated vibrational frequencies and IR intensities, shown as black sticks in Figure 7, replicate the experimental


https://dx.doi.org/10.1021/acs.jpca.0c03545
J. Phys. Chem. A 2020, 124, 5856−5870

spectrum in significant detail and corroborate our preliminary assignments. The structure corresponding to these calculated frequencies, with an f/$\pi$/C12/C8 H-bonding pattern, is shown in Figure 8a. We see that the C-terminal portion adopts the

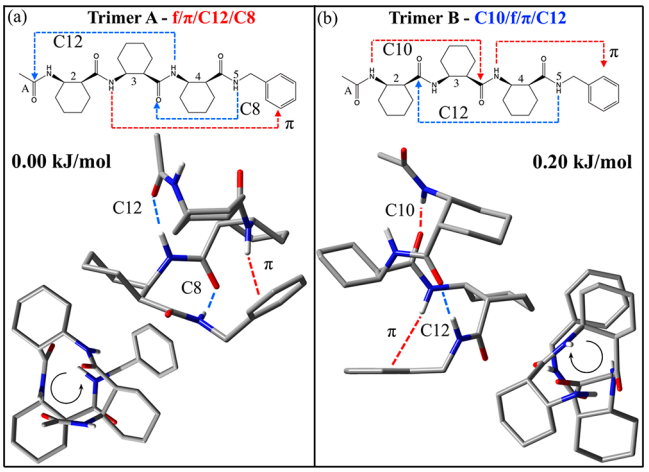


**Figure 8.** Assigned structure and relative zero-point-corrected potential energies of (a) conformer A and (b) conformer B of the trimer. 3D structure and 2D hydrogen-bonding schematics are presented for each molecule, along with a down-axis view from N to the C terminus, highlighting the preferred screw sense of each conformer.

cap-disrupted motif of the LL-dimer with its NH[5]···O=C[3] C8 and NH[3]···$\pi$ interactions, while the N-terminal addition of the ACHC[2] unit gives rise to the NH[4]···O=C[A] C12 H-bond characteristic of the left-handed 12/10-helix. This structural progression implies the emergence of a preferred secondary structure. As seen in the energy level diagram in Figure 5b, this conformer is predicted by the calculations to be the global minimum for the trimer. This conformer forms one full turn of a left-handed 12/10-helix, not including the cap-disrupted portion, that is held together by a single C12 hydrogen bond. We henceforth refer to this secondary structure as a cap-disrupted left-handed 12/10-helix. It is worth noting that if, instead of the cap-disrupted portion, this conformer adopted a C10 H-bond between NH[2] and C=O[4], approximately 1.5 turns of a "pure" left-handed 12/10-helix would be formed.

The amide I and II data of conformer A also show a striking similarity with that of the LL-dimer (shown in Figure 6). Furthermore, the calculated spectrum for conformer A matches the experimental spectrum in significant detail. The high-frequency amide I bands at 1698 and 1690 cm$^{-1}$ correspond to the in-phase and out-of-phase stretches of the C=O[A,2] oscillators. The relative intensities of these bands can be understood by the fact that, in the assigned structure, these groups are nearly antiparallel with one another, rendering the net change in the dipole in the out-of-phase stretch negligible compared with that of the in-phase combination. The two lower frequency bands at 1679 and 1655 cm$^{-1}$ are assigned to C=O[4] and C=O[3], respectively. The relative frequencies of these bands are in keeping with our general expectation that carbonyl groups involved in stronger H-bonded interactions shift to lower frequencies. The assigned amide II transitions display the inverse pattern here, with the NH[4,5] coupled bends appearing at 1568 and 1547 cm$^{-1}$, and the NH[2,3] coupled bends accounting for the transitions at 1522 and 1515 cm$^{-1}$.

*III.C.3. Conformer B.* While experimental conditions were not sufficient to record IR data of this minor conformer of the trimer (conformer B), spectral and computational evidence points to its tentative structural assignment. The UV data show the $S_0$−$S_1$ origin at 37 263 cm$^{-1}$, with Franck−Condon progressions up to $\nu$ = 2, 2, and 1 in vibrations of frequency 54, 188, and 151 cm$^{-1}$, respectively. Vibrational analysis of the tentatively assigned structure (details given presently) shows that each of these modes involve the rocking of the phenyl group against ACHC[3] and NH[4], with the 54 cm$^{-1}$ mode exhibiting the exact same motion as the 54 cm$^{-1}$ mode in the RR-dimer. The UV absorption frequencies match those of the RR-dimer and conformer A of the tetramer (see next section), both of which are right-handed 12/10-helices. Additionally, the IR−UV HB frequency of 3322 cm$^{-1}$ is where absorption of NH[5] in a C12 H-bond occurs, as seen in the IR spectra of

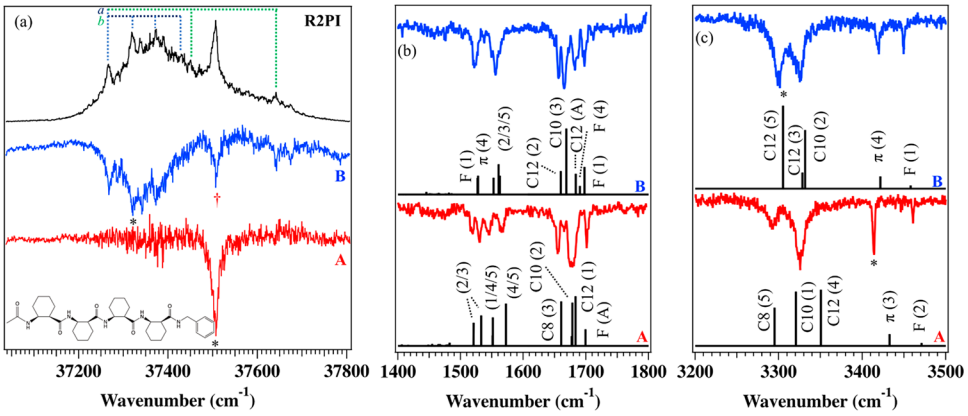


**Figure 9.** (a) R2PI (black) and IR−UV HB spectra in the $S_0$−$S_1$ region of conformer B (blue trace) and conformer A (red trace) of the tetramer. The Franck−Condon progressions marked with *a* and *b* correspond to low-frequency modes of 187 and 54 cm$^{-1}$, respectively, in conformer B. The transition marked with a red dagger in the IR−UV HB spectrum of conformer B represents contamination from conformer A due to overlapping IR frequencies. (b) and (c) RIDIR spectra of conformer B (blue) and A (red) in the amide I/II and hydride stretch regions, respectively. Stick spectra below each experimental trace depict the scaled, harmonic normal-mode frequencies of the assigned conformation. These vibrational transitions, calculated at the B3LYP-D3BJ/6-31+G(d) level of theory, are labeled with the main carrier(s) of the vibration. Transitions marked with an asterisk were those used to collect hole-burn spectra.



https://dx.doi.org/10.1021/acs.jpca.0c03545
J. Phys. Chem. A 2020, 124, 5856−5870

the RR-dimer and conformer A of the tetramer. Finally, the energy level diagram in Figure 5b reveals a second lowest energy conformer that is only 0.2 kJ/mol above the global minimum, with a hydrogen bonding pattern of C10/f/$\pi$/C12, making it the natural intermediate structure in the trimer that links the right-handed 12/10-helix of the RR-dimer with conformer A of the tetramer. This assignment is further substantiated by the calculated IR spectra of this structure, which predicts absorption of the NH[5,2] groups in the C12 and C10 hydrogen bonds at 3316 and 3322 cm$^{-1}$, respectively, which very likely accounts for the IR absorption of this conformer at 3322 cm$^{-1}$ (see Figure S12 for the calculated IR spectra of conformer B).

Figure 8b presents the structure tentatively assigned to conformer B. Comparison of this structure with that of the RR-dimer reveals a striking similarity. Indeed, as was the case when comparing Tri(A) and the LL-dimer, the same structural motif present in the RR-dimer is incorporated in the common C-terminal component of Tri(B). The structure comprises approximately 1.5 turns of a fully formed right-handed 12/10-helix that is held together by single C12 and C10 H-bonds and terminates at the C-terminus with a $\pi$ interaction. We see then, in going from $n$ = 2 to $n$ = 3 of Ac-(ACHC)$_n$-NHBn, two emerging secondary structures; the cap-disrupted left-handed 12/10-helix, and the right-handed 12/10-helix.

**III.D. Tetramer.** *III.D.1. R2PI and IR−UV HB Spectroscopy.* The R2PI and IR−UV HB spectra of the tetramer Ac-(ACHC)$_4$-NHBn are shown in Figure 9a, from which we immediately notice a decrease in spectral resolution due to incomplete cooling of this large molecule following laser desorption, with molecular weight of 649 amu. The result is the presence of sequence and hot bands in the UV spectra. Nevertheless, we are able to identify two unique conformers in the molecular beam.

The IR−UV HB spectrum of conformer B, shown as the blue trace, displays vibronic activity spanning 400 cm$^{-1}$. The peak marked with a red dagger is residual interference from conformer A, due to a small absorption from A at the IR wavelength used for hole-burning (3300 cm$^{-1}$). We note the similarity of this UV spectrum to that of conformer B of the trimer (Figure 7a), and the major conformer of the RR-dimer (Figure 3a). Indeed, we tentatively assign the $S_0$−$S_1$ origin transition of conformer B to the band at 37 265 cm$^{-1}$, approximately the same frequency of conformer B of the trimer. Figure S13 presents a comparative plot of the R2PI spectra of the $n$ = 2−4 series of peptides studied herein. While the spectrum is much less well-resolved than a fully cold counterpart, one can nevertheless still observe several peaks due to Franck−Condon (FC) activity in low-frequency modes. The IR−UV HB spectrum contains FC progressions up to $\nu$ = 3 in 54 cm$^{-1}$ mode and v = 2 in a 187 cm$^{-1}$ mode with each member of the 54 cm$^{-1}$ progression having a smaller peak built off of it with a spacing of 18 cm$^{-1}$. These smaller peaks are likely due either to combination bands with an 18 cm$^{-1}$ vibration in $S_1$, or to $X^1_1$ sequence bands present due to incomplete vibrational cooling, where the corresponding $S_1$ frequency is 18 cm$^{-1}$ larger than in $S_0$. According to vibrational analysis of the assigned structure (see next section), these FC active modes in the tetramer are close analogues of those exhibiting FC progressions in conformer B of the trimer.

The IR−UV HB spectrum of conformer A is shown as the red trace in Figure 9a. In striking contrast to the spectrum of conformer B, we observe a single peak with a FWHM of 15 cm$^{-1}$. We note the close similarity of this spectrum to that of conformer A of the trimer, which adopts a cap-disrupted left-handed 12/10-helix. Indeed, conformer A of the tetramer has its $S_0$−$S_1$ origin transition at 37 507 cm$^{-1}$, just 3 cm$^{-1}$ higher than that of Tri(A). The width of the UV peak reflects incomplete cooling in the expansion, consistent with a molecule of this size.

*III.D.2. RIDIR Spectroscopy.* The conformer-specific RIDIR spectra of the two experimentally observed structures of the tetramer are shown in Figure 9b,c in the amide I/II and NH stretch regions, respectively. As with the smaller molecules in this series, the vibrational spectra of all structures calculated at the DFT B3LYP-D3BJ/6-31+G(d) level of theory were compared with experiment. We expect to see the five unique NH and C═O groups give rise to as many fundamental transitions in each of the NH stretch, amide I, and amide II regions.

The NH stretch spectrum of Tet(B) is presented as the blue trace in Figure 9c. We observe two high-frequency transitions at 3449 and 3420 cm$^{-1}$, an asymmetrically broadened peak with a low-frequency shoulder centered at 3325 cm$^{-1}$, and a symmetrically broadened low-frequency peak at 3299 cm$^{-1}$. We note that the NH stretch spectrum of the RR-dimer exhibits a similar intensity and frequency pattern to that observed here (see Figure 3). Additionally, recalling the close similarity of the UV spectra of the tentatively assigned right-handed 12/10 helix of Tri(B) to that of Tet(B) (Figure S13), we tentatively assign the three highest frequency peaks to a free, a $\pi$-bound, and a C12 hydrogen bonded NH stretch. This leaves assignment of the two remaining low-frequency transitions to what must be NH groups involved in hydrogen bonds of similar strength to the C12 NH group.

Single ACHC residue N-terminal helical growth of the right-handed 12/10-helix of Tri(B) yields one additional C12 hydrogen bonded NH. The calculated stick spectrum of this structure is shown below the experimental trace of Tet(B). We see that it is a match. The excellent agreement between experiment and theory in amides I and II, shown in the top portion of Figure 9b, gives us confidence that the assigned structure, shown in Figure 10a, is indeed a right-handed 12/10-helix, which according to our labeling scheme is f/C10/C12/

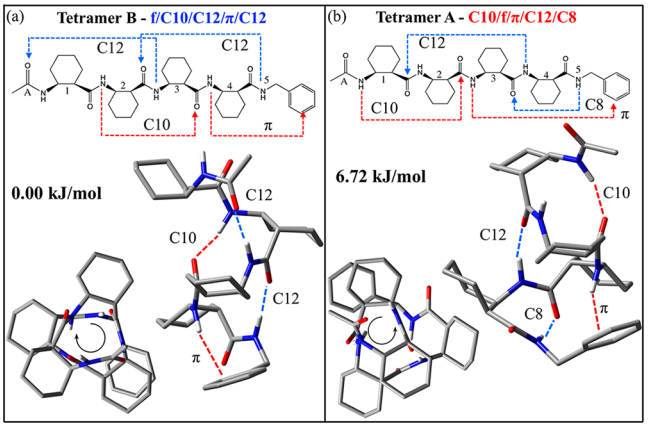


**Figure 10.** Assigned structure and relative zero-point-corrected energies of (a) conformer B and (b) conformer A of the tetramer. 3D structure and 2D hydrogen-bonding schematics are presented for each molecule, along with a down-axis view from N to the C terminus, highlighting the preferred screw sense of each conformer.



https://dx.doi.org/10.1021/acs.jpca.0c03545
J. Phys. Chem. A 2020, 124, 5856−5870

Table 2. Relative Energies and Backbone Dihedral Angles for All Assigned Structures[a]

| | | ACHC$_1$ (*SR*) | | | ACHC$_2$ (*SR*) | | | ACHC$_3$ (*SR*) | | | ACHC$_4$ (*SR*) | | | |
|---|---|---|---|---|---|---|---|---|---|---|---|---|---|---|
| | $\Delta E$ (kJ/mol) | $\varphi_1$ (deg) | $\theta_1$ (deg) | $\psi_1$ (deg) | $\varphi_2$ (deg) | $\theta_2$ (deg) | $\psi_2$ (deg) | $\varphi_3$ (deg) | $\theta_3$ (deg) | $\psi_3$ (deg) | $\varphi_4$ (deg) | $\theta_4$ (deg) | $\psi_4$ (deg) | CNCC (deg) |
| dimer f/$\pi$/C12 | 0.00 | | | | | | | −96 | 50.1 | 102 | 95 | 53 | −102 | −89 |
| R-dimer f/$\pi$/C12 | 0.00 | | | | | | | −96 | 51 | 102 | 94 | 53 | −102 | −89 |
| RR-dimer f/$\pi$/C12 | 0.00 | | | | | | | −95 | 50 | 102 | 94 | 53 | −101 | −89 |
| trimer B C10/f/$\pi$/C12 | 0.20 | | | | 87 | 57 | −72 | −110 | 51 | 81 | 114 | 114 | −101 | −90 |
| tetramer B f/C10/C12/$\pi$/C12 | 0.00 | −116 | 52 | 83 | 107 | 57 | −114 | −101 | 51 | 97 | 99 | 54 | −99 | −89 |
| right-handed 12/10- helix[b] | | −96 | 52 | 95 | 98 | 54 | −92 | −96 | 52 | 95 | 98 | 54 | −92 | |
| L-dimer $\pi$/C8/C8 | 0.00 | | | | | | | −56 | −47 | 101 | 110 | −63 | −63 | −92 |
| LL-dimer $\pi$/C8/C8 | 0.00 | | | | | | | −56 | −47 | 101 | 110 | −63 | −21 | −92 |
| trimer A f/$\pi$/C12/C8 | 0.00 | | | | 101 | −57 | −97 | −90 | −53 | 122 | 114 | −62 | −21 | −85 |
| tetramer A C10/f/$\pi$/C12/C8 | 6.72 | −85 | −56 | 91 | 100 | −60 | −91 | −94 | −53 | 120 | 114 | −61 | −19 | −84 |
| left-handed 12/10- helix[b] | | −110 | −58 | 98 | 103 | −52 | −87 | −110 | −58 | 98 | 103 | −52 | −87 | |

[a]Structures calculated at the B3LYP-D3BJ/6-31+G(d) level of theory. [b]Crystal structure values taken from ref 6.

$\pi$/C12. It comprises approximately two turns of a fully formed right-handed 12/10-helix that is held together by two C12 hydrogen bonds (pointing N → C-terminal) and one C10 hydrogen bond (pointing C → N-terminal), capped at the C-terminus with a $\pi$-interaction. The dihedral angles for this structure, and all structures reported herein, are found in Table 2. The fact that this structure is calculated to be the global minimum among all calculated structures adds further confidence to the assignment (Figure 5b).

The frequency ordering of the amide I bands reflects the strengths of the hydrogen bonds of which the carbonyl groups are a part, as revealed by the relative frequencies of the assigned NH stretch transitions. The two free C═O stretch transitions occurs near 1700 cm$^{-1}$ while the triplet of transitions at 1684 (C12[A]), 1669 cm$^{-1}$ (C10[3]), and 1660 cm$^{-1}$ (C12[2]) reflect an increasing strength of the H-bonds to each C═O group. The relative frequencies of the amide II bands report the same information, but with the frequency pattern inverted. The more weakly bound $\pi$ and free NH bends appear at 1522 cm$^{-1}$, while C10 and C12 NH bends appear as a coupled set of peaks centered at 1556 cm$^{-1}$. In addition to the NH stretch region, the amide I and II spectra of Tet(B) and the RR-dimer are also quite similar to one another, as one might expect of molecules sharing a common secondary structure.

The NH stretch spectra of Tet(A) is shown as the red trace in Figure 9c. We notice the striking similarity of this spectrum to that of Tri(A), the cap-disrupted left-handed 12/10-helix (Figure 7). Recalling the near identical UV spectra of these conformers, we tentatively assign the two high-frequency transitions at 3461 and 3414 cm$^{-1}$ to free and $\pi$-bound NH groups, respectively, the lowest frequency transition at 3292 cm$^{-1}$ to a C8 H-bond, and the 11 cm$^{-1}$ FWHM peak at 3326 cm$^{-1}$ to a C12 H-bond. There seem to be no experimental peaks left to assign. However, single ACHC residue N-terminal helical growth of the cap-disrupted left-handed 12/10-helix of Tri(A) would give rise to an additional C10 hydrogen bonded NH. We note that the integrated intensity of the assigned C12 transition in Tet(A) is nearly double that of the analogous peak in Tri(A). On this basis, we postulate that two unique NH stretch fundamentals contribute to the peak's unusually large intensity.

The calculated stick spectra of the cap-disrupted left-handed 12/10-helix tetramer is shown below the experimental trace of Tet(A). The match with experiment is good in the NH stretch region, and excellent in the amide I/II regions (Figure 9b). As was the case with Tet(B), the amide I and II data generally reflect the hydrogen bond strengths as revealed through their relative frequencies in the NH stretch spectrum. The calculated vibrational spectra in the NH and amide I/II regions corresponding to other low-energy conformers of the tetramer, including the "pure" left-handed 12/10 helix, are presented under the experimental trace of conformer A in Figure S14.

This structure is calculated to be the second lowest energy conformer, with energy 6.72 kJ/mol above Tet(B), giving us further confidence in its assignment. The assigned structure, shown in Figure 10b, is the cap-disrupted left-handed 12/10-helix, labeled as C10/f/$\pi$/C12/C8. It comprises approximately 1.5 turns of a left-handed 12/10-helix (not including the cap-disrupted portion), which is held together by counter-propagating C12 and C10 hydrogen bonds.

## IV. DISCUSSION

Through conformation-specific IR spectroscopy in the hydride stretch and amide I/II regions, along with corroborating spectral and computational evidence, we have determined the intrinsic conformational preferences of a series of cyclically constrained $\beta$-peptides in the gas-phase. We have shown that the gas-phase conformer population contains both left- and right-handed 12/10-mixed helical structures for Ac-(ACHC)$_n$-NHBn with $n$ = 2, 3, 4. As shown in Figure 5, the observed conformation is the global minimum calculated structure in each case, with the remaining assigned structures being the next lowest energy structure in all but one case (dimer). These results give us confidence that the B3LYP-D3BJ/6-31+G(d) level of theory accurately characterizes the conformational energetics of these molecules. With this in mind, we now turn to a discussion of the energy landscapes of these increasingly complex $\beta$-peptides, beginning with the dipeptides.

**IV.A. Dipeptides.** *IV.A.1. Steric Control of Helical Handedness in the Dipeptides.* One of the goals of this study was to determine the effect that the methylated ACHC residues would have on directing formation of a particular helical screw sense in the isolated gas-phase molecule. Choi



https://dx.doi.org/10.1021/acs.jpca.0c03545
J. Phys. Chem. A 2020, 124, 5856−5870

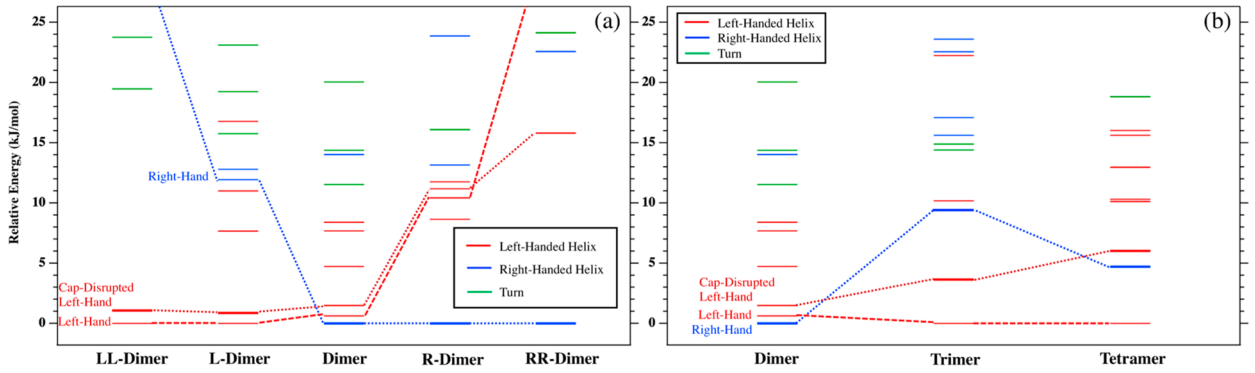


**Figure 11.** Energy level diagrams for (a) the set of methylated dipeptides and (b) the series Ac-$(ACHC)_n$-NHBn with $n$ = 2, 3, 4, upon replacing the C-terminal NHBn cap with NHMe. Each conformational minima has its relative zero-point-corrected energy (B3LYP-D3BJ/6-31+G(d)) plotted as a horizontal bar and color-coded to represent left-handed (red), right-handed (blue), or general turned (green) structures. Experimentally assigned conformers are represented with a heavy horizontal bar. The "pure" right- and left-handed helices as well as the cap-disrupted helical structures are labeled and connected via dotted lines to their corresponding structures across the molecules.

and co-workers have demonstrated that incorporation of an L- or R-ACHC group at every other residue in *t*-BuO-$(ACHC)_n$-NHMe with $n$ = 4, 5, is sufficient to lock the conformation into either the left- or right-handed 12/10-helix in solution.[6,7] We explore here what effect incorporating one or two such methylated residues has on the conformational preferences and energy landscape of the isolated, gas-phase dipeptide.

We now return to Figure 5a, which shows the zero-point corrected energies of all the gas-phase structures calculated to lie within 25 kJ/mol of the global minimum for each dipeptide. We have seen that all of the assigned conformations fall into one of two categories: emergent forms of either the right-handed 12/10-helix (f/$\pi$/C12) or the cap-disrupted left-handed 12/10-helix ($\pi$/C8/C8). We have labeled the lowest energy structure corresponding to these conformational families, as well as the pure left-handed 12/10-helix conformation (C10/f/f), for each unique molecule. Its energetic path upon ACHC methylation is traced with dotted lines.

Note, first, that the number of low-energy structures present in the dipeptides decreases as more methylated ACHC units are added, thereby increasing steric constraints. The dominant conformation of the dimer is the right-handed helix (0.0 kJ/mol) while the minor conformation is tentatively assigned to the cap-disrupted left-handed helix (11.6 kJ/mol). The 10.4 kJ/mol separation of the global minimum from the next lowest energy structure constitutes a strong energetic preference for the right-handed 12/10-helix. This preference persists with the addition of one and two methyl groups in the R-dimer and RR-dimer with energy separations of 13.2 and 18.4 kJ/mol, respectively. This large separation in the RR-dimer between the global minimum and second lowest energy structure is unprecedented in short peptides or synthetic foldamers.

N-terminal substitution of the dimer's ACHC[3] with L-ACHC (L-dimer) inverts this trend, where all population is now funneled into the cap-disrupted left-handed 12/10-helix, which is the minor conformer of the unsubstituted dimer. Additional L-ACHC substitution of ACHC[4] (LL-dimer) locks in this structure, where the energy separation between the assigned global minimum structures and the next lowest energy conformers is ~7.5 kJ/mol in each case. The smaller energy gap in L(L)- compared to R(R)-dipeptides, when combined with the clear preference for the right-handed helix in the dimer, point clearly to the inherent bias of the unmethylated ACHC unit to forming a right-handed helix.

Although not experimentally observed, the pure left-handed 12/10-helix (C10/f/f) is calculated as a low-energy structure for the L(L)-dipeptides and the dimer. We return to this point momentarily. These calculated results, along with our experimentally assigned conformations, lead one to conclude that selectively methylating ACHC residue(s) is sufficient to drive population exclusively into one particular screw sense over the other under isolated, gas-phase conditions.

*IV.A.2. Effects of the C-Terminal NHBn Cap in the Dipeptides.* Zero-point corrected energy calculations were also performed on the pool of structures where the sterically intrusive C-terminal NHBn cap was replaced with an NHMe cap, to assess how the energies of the structures might change in the phenyl ring's absence. The results for the NHMe capped dipeptides are shown in Figure 11a. We immediately notice a sharp decrease in the number of structural minima for each dipeptide. This is due to the removal of all near-redundant phenyl rotamer structures, which all funnel into the same conformational minima upon NHMe substitution of the NHBn cap.

Focusing our attention on the right-handed helix former (blue), we see that the relative energies in going from the LL-dimer to the RR-dimer follow the same trend as its NHBn counterpart (Figure 5a), where it is the global energy minimum structure in the dimer, R-dimer, and RR-dimer, but then sharply increases in energy with each L-ACHC addition. In the case of LL-dimer, the loss of the $\pi$-interaction greatly destabilizes this structure with respect to both left-handed helices.

Upon NHMe capping, the pure left-handed 12/10-helix displaces the cap-disrupted 12/10-helix (f/C8/C8) as the global minimum structure for both the L- and LL-dimers. At the dimer level, both the pure and cap-disrupted helices are substantially more stable relative to their NHBn counterparts, with energies of 0.62 and 1.48 kJ/mol, respectively (compared with 10.36 and 11.62 kJ/mol). The preference for the pure left-handed helix in the NHMe-capped L(L)-dimers highlights the perturbative impact that $\pi$-interactions may have on preferred structure in the gas-phase. The calculations thus predict that in the absence of the C-terminal phenyl ring, the structures that we experimentally assigned to the cap-disrupted left-handed 12/10-helix would funnel their population into the "pure" left-


https://dx.doi.org/10.1021/acs.jpca.0c03545
J. Phys. Chem. A 2020, 124, 5856−5870

handed helix. Finally, the fact that the pure left- and right-handed 12/10 mixed helices are nearly isoenergetic with C-terminal NHMe capping supports the notion that the $(ACHC)_2$ unit may be regarded as achiral.

**IV.B. Ac-(ACHC)$_n$-NHBn, $n$ = 2, 3, 4.** *IV.B.1. Potential Energy Landscapes for Ac-(ACHC)$_n$-NHBn, $n$ = 2, 3, 4.* Another major goal of this study was to determine which screw sense, if any, emerges in unmethylated ACHC oligomers as a function of increasing length. We have experimentally determined that for $n$ = 2−4 in Ac-$(ACHC)_n$-NHBn, both the right-handed 12/10-helix and the cap-disrupted left-handed 12/10-helical structures are adopted. However, the spectroscopy also points to an alternating preference with oligomer length. Using integrated vibronic transition intensities as a first-order approximation of relative abundances, the right-handed 12/10-helix is the major conformer when $n$ = 2 and 4, while the cap-disrupted left-handed 12/10-helix is the major conformer at $n$ = 3. Energetic analysis, given presently, corroborates this assessment. Possible reasons for these asymmetric distributions are given in section IV.C.

We refer again to Figure 5b, which presents the calculated zero-point corrected energies of all structures within 25 kJ/mol of the global minimum for the unmethylated dimer, trimer, and tetramer. As was the case with the dipeptides, the secondary structures of all minima fall into one of three color-coded categories: left-handed helix (red), right-handed helix (blue), and turned structures (green). The lowest energy structures corresponding to the right-handed, cap-disrupted left-handed, and pure left-handed 12/10-helices are labeled in the figure, with the energetic path accompanying the addition of each N-terminal ACHC unit traced with dotted lines.

The number of low-energy structures remains nearly constant across the dimer (20), trimer (23), and tetramer (18). This is in contrast to a previous gas-phase study from some of us of the flexible Z-Gly$_n$-OH series ($n$ = 1−3, 5), where the number of calculated minima increased in going from $n$ = 1 to $n$ = 3 and then sharply decreased in going from $n$ = 3 to $n$ = 5.[37] In that series of molecules, it was the number of hydrogen bonds present in the structure that conferred stability. At $n$ = 5, fewer structures existed that maximized the number of hydrogen bonds. In our series of much more rigid molecules, the number of distinct conformational families remains nearly constant in going from $n$ = 2 to $n$ = 4, because the addition of one or two ACHC units to the N-terminus simply grows and expands upon the existing secondary structures found in the dimer manifold.

*IV.B.2. . Effects of the C-Terminal NHBn Cap for Ac-(ACHC)$_n$-NHBn, n = 2, 3, 4.* Figure 11b presents the relative, zero-point corrected energies of the low-energy conformers of the dimer, trimer, and tetramer upon replacement of the NHBn cap with a less intrusive NHMe cap. As with the dipeptides (Figure 11a), there is a sharp decrease in the number of low-energy conformers available to each molecule due to the removal of conformers differing only in its phenyl rotamer.

In the dimer, the three main helical motifs are close in energy, with the right-handed helix remaining the global energy minimum. At the trimer level, the right-handed helix is destabilized by 9.37 kJ/mol relative to the pure left-handed helix, which displaced the cap-disrupted helix as the global minimum. At the tetramer level, the right-handed helix is now the second lowest energy structure at 4.71 kJ/mol above the pure left-handed helix, which has moved from third lowest energy to the global minimum. These results suggest that the cap-disrupted left-handed 12/10-helical structures that we experimentally observed in the dimer, trimer, and tetramer would likely funnel their population into the pure left-handed 12/10-helix upon capping with the more biologically relevant NHMe group, resulting in a distribution of "pure" left- and right-handed 12/10 helices. Additionally, the fact that the energy separation decreases between the pure left- and right-handed helices in Ac-$(ACHC)_n$-NHMe when $n$ is even is consistent with the $(ACHC)_2$ dimer unit as an achiral building block.

**IV.C. The ACHC Residue Is a Robust Left- and Right-Handed 12/10 Mixed-Helix Former.** *IV.C.1. Conservation of Secondary Structure between Phases.* It is striking that the seven molecules studied in this work funnel their population into only two unique conformational families: the pure right-handed 12/10 mixed-helix and the cap-disrupted left-handed 12/10 mixed-helix. We have reasoned in the previous sections that in the absence of the NHBn cap it is very likely that the cap-disrupted left-handed helix population would be funneled into the pure left-handed 12/10 helix. With this in mind, in this section we compare these gas-phase structures with their analogous solution and crystal phase structures.

In solution, the left- and right-handed helices interconvert on the NMR time scale between one another via the cooperative inversion of all ACHC residues from one chair conformation to the other.

The exquisite sensitivity of the helical preference to environmental effects is apparent when one compares the structures observed in crystalline form. X-ray structures derived from crystals of the *t*-BuO/NHMe capped tetramer show it to adopt a right-handed 12/10 mixed-helix, while the X-ray structure of Ac/NHBn capped tetramer is a left-handed 12/10 mixed-helix.[7] The change in helical handedness in the solid state crystals of such similar molecules must be attributed to crystal packing effects, where intermolecular interactions play a key role in tipping conformational preferences toward one helix or another. Finally, we note that the pentamer member of our Ac/NHBn series adopts a left-handed 12/10 helix when crystallized.[6]

Our experimental determination that both left- and right-handed helices exist in the gas phase at the dimer, trimer, and tetramer levels occurs despite the fact that we are laser desorbing the solid, which we have just argued is of one handedness in crystalline form. Two scenarios may occur. Either laser desorption takes a single-handed helical solid into the gas phase with sufficient energy that it can partially interconvert before being cooled by supersonic expansion, or the sample itself is not of a single-handed helix, since they were not prepared in crystalline form.

We test the first hypothesis based on the calculations. Laser desorption temperatures are not well characterized, with some studies suggesting that temperatures in the initial desorption plume may reach as high as 700 K.[41,42] In a previous study we calculated the isomerization rate of an $\alpha\beta\alpha$-tripeptide system involving single ACHC ring isomerization from one chair conformation to the other.[24] At an estimated laser-desorption temperature of 300 K, we determined that the rate limiting ring-flipping step occurred 3 orders of magnitude slower than the collisional cooling rate in the supersonic expansion, rendering desorption-induced isomerization very unlikely. In the simplest case of the ACHC dimer, one would require two ACHC rings to flip, the rate of which is significantly slower


https://dx.doi.org/10.1021/acs.jpca.0c03545
J. Phys. Chem. A 2020, 124, 5856−5870

than for the single ACHC tripeptide. Therefore, we conclude that it is far more likely that our solid-state samples contain both handed helices, which we laser desorb and subsequently detect in the gas-phase.

*IV.C.2. Free Energy Considerations and Structural Implications.* We have calculated the free energies of all conformers in the present series of seven molecules calculated to lie within 50 kJ/mol of zero-point corrected relative energy (Supporting Information). Assuming thermal equilibrium at a laser desorption temperature of 300 K, we can use the free energy calculations to predict the initial populations prior to cooling. In all seven molecules studied herein, the free energy trends mirror the potential energy trends quite closely. This is an interesting result, which points to the steric constraints of the ACHC ring along the peptide backbone preventing extended conformations from forming. Since these extended conformations typically possess a greater number of low-frequency modes, they grow in thermal population with temperature. The steric constraints of the ACHC residue effectively reduce the role of entropy in determining the conformational makeup. These free energy trends, in conjunction with the preservation of structure across the solution, crystal, and gas-phase, imply that poly-ACHC is a robust 12/10 mixed-helical former that is to a large degree impervious to local environment.

## V. CONCLUSIONS

The conformational preferences of a series of cyclically constrained $\beta$-peptide foldamers were characterized in the gas-phase using single-conformation, IR−UV double resonance laser spectroscopy. At every size in the series Ac-$(ACHC)_n$-NHBn, $n$ = 2, 3, 4, two emergent secondary structures are observed: the right-handed 12/10 mixed helix and the cap-disrupted left-handed 12/10 mixed helix. DFT calculations predict that substitution of the intrusive C-terminal NHBn cap by a more natural NHMe cap will result in the pure left-handed 12/10 mixed helix displacing the cap-disrupted left-handed 12/10 helix as a populated, low-energy conformer.

We also investigated whether methylation at strategic sites in the cyclohexane backbone is an effective means of directing the helical sense preferred by the $\beta$-peptide. Already at the dipeptide ($n$ = 2) level, our experimental results indicate that a single methylated residue is sufficient to shift all population into one screw sense or the other. Furthermore, computational results indicate that double methylation increases the energetic stability of the intended helical structure with respect to all other conformations.

In future studies, it would be interesting to characterize ACHC oligomers containing more than four residues, to test whether the emerging secondary structures remain the preferred conformation at even greater lengths. Such longer helices should also exhibit growing evidence of cooperative strengthening of the H-bonds within the helix.

These gas phase results indicate that even in the absence of solvent, the 12/10 mixed helix is a robust secondary structure that oligomers of the ACHC residue prefer in both the condensed phase and the vacuum. The similarity in calculated free and potential energies of this series of molecules is almost certainly due to the highly sterically constrained nature of the ACHC residue. The lack of flexibility exhibited by members of such a highly constrained $\beta$-peptide building block could be a desirable trait when engineering foldamer-based drugs, which must adopt a particular secondary structure in both hydrophobic and hydrophilic environments. Additionally, the achirality of the "pseudosymmetric" $(ACHC)_2$ unit, which gives rise to the dynamic handed helices in certain environments, may be further constrained by ACHC methylation in situations where a single handedness is preferred over dynamic handedness.

Finally, having determined that both left- and right-handed 12/10-helices are present in these samples, IR-population transfer studies could be used to study their interconversion (or lack thereof).[43,44] Such studies would be complicated by the requirement to IR excite in the same region as laser desorption occurs. Furthermore, laser desorption from a known, single-crystal sample would provide further insight to the role played by the molecular solid in determining the observed conformations in the gas phase.

## ■ ASSOCIATED CONTENT

### Supporting Information

The Supporting Information is available free of charge at https://pubs.acs.org/doi/10.1021/acs.jpca.0c03545.

Synthetic methods and characterization data, laser desorption details, mass spectra, UV and IR spectra of R- and RR-dimers, structure and calculated IR spectra of turned structures at the $n$ = 2−4 level, UV and IR spectra of L-dimer, R2PI spectra of all dipeptides, calculated IR spectrum of trimer conf B, R2PI spectra of $n$ = 2−4 main series molecules, calculated IR spectra of low-lying conformers of the tetramer compared with spectrum of conf A, free and potential energies of all molecules, Z-$Gly_n$−OH vs Ac-$ACHC_n$-NHBn comparison (PDF)

## ■ AUTHOR INFORMATION


### Corresponding Authors

**Soo Hyuk Choi** − *Department of Chemistry, Yonsei University, Seoul 03722, Korea;* orcid.org/0000-0003-4066-6504; Email: sh-choi@yonsei.ac.kr

**Timothy S. Zwier** − *Department of Chemistry, Purdue University, West Lafayette, Indiana 47907-2084, United States;* orcid.org/0000-0002-4468-5748; Email: tszwier@sandia.gov

### Authors

**Karl N. Blodgett** − *Department of Chemistry, Purdue University, West Lafayette, Indiana 47907-2084, United States;* orcid.org/0000-0002-6827-0328

**Geunhyuk Jang** − *Department of Chemistry, Yonsei University, Seoul 03722, Korea*

**Sojung Kim** − *Department of Chemistry, Yonsei University, Seoul 03722, Korea*

**Min Kyung Kim** − *Department of Chemistry, Yonsei University, Seoul 03722, Korea*

Complete contact information is available at: https://pubs.acs.org/10.1021/acs.jpca.0c03545


### Notes

The authors declare no competing financial interest.

## ■ ACKNOWLEDGMENTS

G.J., S.K., M.K.K. and S.H.C. acknowledge support from the National Research Foundation of Korea (NRF-

2019R1H1A2080002) and Yonsei University. K.N.B. and T.S.Z. gratefully acknowledge support for this research from the National Science Foundation Chemical Structure, Dynamics & Mechanisms A program under grant CHE-1764148.

## REFERENCES

(1) Gord, J. R.; Walsh, P. S.; Fisher, B. F.; Gellman, S. H.; Zwier, T. S. Mimicking the First Turn of an α-Helix with an Unnatural Backbone: Conformation-Specific IR and UV Spectroscopy of Cyclically Constrained β/γ-Peptides. *J. Phys. Chem. B* **2014**, *118* (28), 8246−8256.
(2) Choi, S. H. Helical Structures of Unnatural Peptides for Biological Applications. *Biomed. Eng. Lett.* **2013**, *3* (4), 226−231.
(3) Crisma, M.; Formaggio, F.; Moretto, A.; Toniolo, C. Peptide Helices Based on α-Amino Acids. *Biopolymers* **2006**, *84* (1), 3−12.
(4) Barlow, D.; Thornton, J. Helix geometry in proteins. *J. Mol. Biol.* **1988**, *201* (3), 601−619.
(5) Le Bailly, B. A.; Clayden, J. Dynamic foldamer chemistry. *Chem. Commun.* **2016**, *52* (27), 4852−4863.
(6) Shin, S.; Lee, M.; Guzei, I. A.; Kang, Y. K.; Choi, S. H. 12/10-Helical β-Peptide with Dynamic Folding Propensity: Coexistence of Right-and Left-handed Helices in an Enantiomeric Foldamer. *J. Am. Chem. Soc.* **2016**, *138*, 13390.
(7) Jang, G.; Shin, S.; Guzei, I. A.; Jung, S.; Choi, M.-G.; Choi, S. H. Crystal Packing-induced Dimorphism of 12/10-Helical β-Peptides with Dynamic Folding Propensity. *Bull. Korean Chem. Soc.* **2018**, *39* (2), 265−268.
(8) Banno, M.; Yamaguchi, T.; Nagai, K.; Kaiser, C.; Hecht, S.; Yashima, E. Optically active, amphiphilic poly (meta-phenylene ethynylene) s: synthesis, hydrogen-bonding enforced helix stability, and direct AFM observation of their helical structures. *J. Am. Chem. Soc.* **2012**, *134* (20), 8718−8728.
(9) Maeda, K.; Yashima, E. Dynamic helical structures: detection and amplification of chirality. In *Supramolecular Chirality*; Springer, 2006; pp 47−88.
(10) Ke, Y. Z.; Nagata, Y.; Yamada, T.; Suginome, M. Majority-Rules-Type Helical Poly (quinoxaline-2, 3-diyl) s as Highly Efficient Chirality-Amplification Systems for Asymmetric. *Angew. Chem., Int. Ed.* **2015**, *54* (32), 9333−9337.
(11) Dawson, S. J.; Mészáros, Á.; Pethő, L.; Colombo, C.; Csékei, M.; Kotschy, A.; Huc, I. Controlling Helix Handedness in Water-Soluble Quinoline Oligoamide Foldamers. *Eur. J. Org. Chem.* **2014**, *2014* (20), 4265−4275.
(12) Seebach, D.; Matthews, J. L. β-Peptides: a surprise at every turn. *Chem. Commun.* **1997**, No. 21, 2015−2022.
(13) Gellman, S. H. Foldamers: A Manifesto. *Acc. Chem. Res.* **1998**, *31* (4), 173−180.
(14) Cheng, R. P.; Gellman, S. H.; DeGrado, W. F. β-Peptides: From Structure to Function. *Chem. Rev.* **2001**, *101* (10), 3219−3232.
(15) Seebach, D.; Hook, D. F.; Glättli, A. Helices and Other Secondary Structures of β- and γ-Peptides. *Biopolymers* **2006**, *84* (1), 23−37.
(16) Seebach, D.; Gardiner, J. β-Peptidic Peptidomimetics. *Acc. Chem. Res.* **2008**, *41* (10), 1366−1375.
(17) Horne, W. S.; Gellman, S. H. Foldamers with Heterogeneous Backbones. *Acc. Chem. Res.* **2008**, *41* (10), 1399−1408.
(18) Johnson, L. M.; Gellman, S. H. Chapter Nineteen - α-Helix Mimicry with α/β-Peptides. In *Methods Enzymol.*; Keating, A. E., Ed.; Academic Press, 2013; Vol. *523*, pp 407−429.
(19) Hamuro, Y.; Schneider, J. P.; DeGrado, W. F. De Novo Design of Antibacterial β-Peptides. *J. Am. Chem. Soc.* **1999**, *121* (51), 12200−12201.
(20) Werder, M.; Hauser, H.; Abele, S.; Seebach, D. β-Peptides as Inhibitors of Small-Intestinal Cholesterol and Fat Absorption. *Helv. Chim. Acta* **1999**, *82* (10), 1774−1783.
(21) Simpson, G. L.; Gordon, A. H.; Lindsay, D. M.; Promsawan, N.; Crump, M. P.; Mulholland, K.; Hayter, B. R.; Gallagher, T. Glycosylated foldamers to probe the carbohydrate− carbohydrate interaction. *J. Am. Chem. Soc.* **2006**, *128* (33), 10638−10639.
(22) Mándity, I. M.; Fülöp, L.; Vass, E.; Tóth, G. K.; Martinek, T. A.; Fülöp, F. Building β-peptide H10/12 foldamer helices with six-membered cyclic side-chains: fine-tuning of folding and self-assembly. *Org. Lett.* **2010**, *12* (23), 5584−5587.
(23) Choi, S. H.; Ivancic, M.; Guzei, I. A.; Gellman, S. H. Structural Characterization of Peptide Oligomers Containing (1R,2S)-2-Amino-cyclohexanecarboxylic Acid (cis-ACHC). *Eur. J. Org. Chem.* **2013**, *2013* (17), 3464−3469.
(24) Blodgett, K. N.; Zhu, X.; Walsh, P. S.; Sun, D.; Lee, J.; Choi, S. H.; Zwier, T. S. Conformer-Specific and Diastereomer-Specific Spectroscopy of αβα Synthetic Foldamers: Ac−Ala−βACHC−Ala−NHBn. *J. Phys. Chem. A* **2018**, *122*, 3697.
(25) Appella, D. H.; Christianson, L. A.; Karle, I. L.; Powell, D. R.; Gellman, S. H. β-Peptide Foldamers: Robust Helix Formation in a New Family of β-Amino Acid Oligomers. *J. Am. Chem. Soc.* **1996**, *118* (51), 13071−13072.
(26) Wu, Y.-D.; Han, W.; Wang, D.-P.; Gao, Y.; Zhao, Y.-L. Theoretical Analysis of Secondary Structures of β-Peptides. *Acc. Chem. Res.* **2008**, *41* (10), 1418−1427.
(27) Baldauf, C.; Günther, R.; Hofmann, H.-J. Mixed Helices—A General Folding Pattern in Homologous Peptides? *Angew. Chem., Int. Ed.* **2004**, *43* (12), 1594−1597.
(28) Baldauf, C.; Günther, R.; Hofmann, H.-J. Theoretical Prediction of the Basic Helix Types in α,β-Hybrid Peptides. *Biopolymers* **2006**, *84* (4), 408−413.
(29) Lubman, D. M. Analytical Multiphoton Ionization Mass Spectrometry. Part II. Applications. *Mass Spectrom. Rev.* **1988**, *7* (6), 559−592.
(30) Zwier, T. S. The Spectroscopy of Solvation in Hydrogen-Bonded Aromatic Clusters. *Annu. Rev. Phys. Chem.* **1996**, *47* (1), 205−241.
(31) Mohamadi, F.; Richards, N. G.; Guida, W. C.; Liskamp, R.; Lipton, M.; Caufield, C.; Chang, G.; Hendrickson, T.; Still, W. C. MacroModel—an Integrated Software System for Modeling Organic and Bioorganic Molecules Using Molecular Mechanics. *J. Comput. Chem.* **1990**, *11* (4), 440−467.
(32) Frisch, M.; Trucks, G.; Schlegel, H.; Scuseria, G.; Robb, M.; Cheeseman, J.; Scalmani, G.; Barone, V.; Petersson, G.; Nakatsuji, H. *Gaussian 16*, Revision A; Gaussian, Inc., 2016; Vol. 3.
(33) Grimme, S. Accurate description of van der Waals complexes by density functional theory including empirical corrections. *J. Comput. Chem.* **2004**, *25* (12), 1463−1473.
(34) Grimme, S. Semiempirical hybrid density functional with perturbative second-order correlation. *J. Chem. Phys.* **2006**, *124* (3), 034108.
(35) Gord, J. R.; Hewett, D. M.; Hernandez-Castillo, A. O.; Blodgett, K. N.; Rotondaro, M. C.; Varuolo, A.; Kubasik, M. A.; Zwier, T. S. Conformation-Specific Spectroscopy of Capped, Gas-Phase Aib Oligomers: Tests of the Aib Residue as a 310-Helix Former. *Phys. Chem. Chem. Phys.* **2016**, *18* (36), 25512−25527.
(36) Walsh, P. S.; Dean, J. C.; McBurney, C.; Kang, H.; Gellman, S. H.; Zwier, T. S. Conformation-specific spectroscopy of capped glutamine-containing peptides: role of a single glutamine residue on peptide backbone preferences. *Phys. Chem. Chem. Phys.* **2016**, *18* (16), 11306−11322.
(37) Dean, J. C.; Buchanan, E. G.; Zwier, T. S. Mixed 14/16 Helices in the Gas Phase: Conformation-Specific Spectroscopy of Z-(Gly)n, n = 1, 3, 5. *J. Am. Chem. Soc.* **2012**, *134* (41), 17186−17201.
(38) Fischer, J. L.; Elvir, B. R.; DeLucia, S.-A.; Blodgett, K. N.; Zeller, M.; Kubasik, M. A.; Zwier, T. S. Single-Conformation Spectroscopy of Capped Aminoisobutyric Acid Dipeptides: The Effect of C-Terminal Cap Chromophores on Conformation. *J. Phys. Chem. A* **2019**, *123*, 4178.
(39) Blodgett, K. N.; Fischer, J. L.; Lee, J.; Choi, S. H.; Zwier, T. S. Conformation-Specific Spectroscopy of Asparagine-Containing Peptides: Influence of Single and Adjacent Asn Residues on Inherent Conformational Preferences. *J. Phys. Chem. A* **2018**, *122*, 8762.


https://dx.doi.org/10.1021/acs.jpca.0c03545
J. Phys. Chem. A 2020, 124, 5856−5870

(40) Buchanan, E. G.; James, W. H.; Choi, S. H.; Guo, L.; Gellman, S. H.; Müller, C. W.; Zwier, T. S. Single-conformation infrared spectra of model peptides in the amide I and amide II regions: Experiment-based determination of local mode frequencies and inter-mode coupling. *J. Chem. Phys.* **2012**, *137* (9), 094301.
(41) Maechling, C. R.; Clemett, S. J.; Engelke, F.; Zare, R. N. Evidence for Thermalization of Surface-Desorbed Molecules at Heating Rates of 108 K/s. *J. Chem. Phys.* **1996**, *104* (21), 8768−8776.
(42) Handschuh, M.; Nettesheim, S.; Zenobi, R. Is Laser Heating Advantageous for Thermal Desorption of Large Polar Molecules? *J. Chem. Phys.* **1997**, *107* (7), 2603−2610.
(43) Dian, B. C.; Longarte, A.; Winter, P. R.; Zwier, T. S. The Dynamics of Conformational Isomerization in Flexible Biomolecules. I. Hole-Filling Spectroscopy of N-Acetyl Tryptophan Methyl Amide and N-acetyl Tryptophan Amide. *J. Chem. Phys.* **2004**, *120* (1), 133−147.
(44) Dian, B. C.; Longarte, A.; Zwier, T. S. Conformational Dynamics in a Dipeptide After Single-Mode Vibrational Excitation. *Science* **2002**, *296* (5577), 2369−2373.


https://dx.doi.org/10.1021/acs.jpca.0c03545
*J. Phys. Chem. A* 2020, 124, 5856−5870